frontiers in Chemistry

ORIGINAL RESEARCH
published: 04 October 2018
doi: 10.3389/fchem.2018.00467

Photoluminescence Properties of Layered Perovskite-Type Strontium Scandium Oxyfluoride Activated With Mn^{4+}

Hideki Kato[1]*, *Yohei Takeda*[1], *Makoto Kobayashi*[1], *Hisayoshi Kobayashi*[2] and *Masato Kakihana*[1]

[1] Institute of Multidisciplinary Research for Advanced Materials, Tohoku University, Sendai, Japan, [2] Department of Chemistry and Materials Technology, Graduate School of Science and Technology, Kyoto Institute of Technology, Kyoto, Japan

In this research, we have found that layered perovskite titanate Sr_2TiO_4 doped with Mn^{4+} exhibits photoluminescence even at room temperature despite no luminescence from Mn^{4+}-doped $SrTiO_3$ with a three-dimensional bulky perovskite structure. The relative position of t_{2g} orbital of Mn to the valence band is a key factor for appearance of Mn^{4+}-emission in Sr_2TiO_4:Mn. This result suggested usefulness of layered perovskite-type materials as hosts for Mn^{4+}-activated phosphors than the bulky perovskite-type materials. Our investigation into photoluminescence of Mn^{4+}-doped layered perovskite compounds has revealed that strontium scandium oxyfluoride Sr_2ScO_3F activated with Mn^{4+} exhibits Mn^{4+}-emission with a peak at 697 nm under excitation at 300–600 nm and its emission intensity is much stronger than that of Sr_2TiO_4:Mn. The internal and external quantum yields of Sr_2ScO_3F:Mn were determined to be 50.5 and 43.5% under excitation at 345 nm, respectively.

Keywords: photoluminescence, scandium oxyfluoride, layered perovskite, tetravalent manganese, red emission

OPEN ACCESS

Edited by:
Nobuhito Imanaka,
Osaka University, Japan

Reviewed by:
Tomokatsu Hayakawa,
Nagoya Institute of Technology, Japan
Saburo Hosokawa,
Kyoto University, Japan

***Correspondence:**
Hideki Kato
hideki.kato.e2@tohoku.ac.jp

Specialty section:
This article was submitted to Physical Chemistry and Chemical Physics, a section of the journal Frontiers in Chemistry

Received: *20 July 2018*
Accepted: *18 September 2018*
Published: *04 October 2018*

Citation:
Kato H, Takeda Y, Kobayashi M, Kobayashi H and Kakihana M (2018) Photoluminescence Properties of Layered Perovskite-Type Strontium Scandium Oxyfluoride Activated With Mn^{4+}. Front. Chem. 6:467. doi: 10.3389/fchem.2018.00467

INTRODUCTION

White light emitting diodes (W-LEDs) based on blue-LEDs are widely spreading to various fields as highly efficient solid lightings (Lin et al., 2016; Adachi, 2018; Wang et al., 2018). Artificial white light is basically obtained by combination of blue and yellow light emitted from a blue-LED chip and a yellow-emitting phosphor $Y_3Al_5O_{12}$:Ce, respectively. Such white light is inevitably cool white with high color temperature due to poor emission strength of $Y_3Al_5O_{12}$:Ce in red region. Efficient red-emitting phosphors are added to achieve artificial warm white light by tuning color temperature. Nitride phosphors activated with Eu^{2+} such as (Sr,Ca)$AlSiN_3$:Eu^{2+} and $M_2Si_5N_8$:Eu^{2+} (M = Ca, Sr, and Ba) are extensively studied and commercially used as the red-emitting phosphors (Li et al., 2006, 2009; Uheda et al., 2006; Watanabe and Kijima, 2009; Tsai et al., 2015; Wang et al., 2018). However, requirements of high temperature and high pressure in synthesis of nitrides are drawbacks of nitride phosphors rising the costs. Therefore, development of alternative yellow—to red-emitting phosphors activated with Eu^{2+}, which can be synthesized milder conditions in comparison with nitrides, is also conducted for oxides, phosphates, and oxyhalides (Toda et al., 2006; Daicho et al., 2012, 2018; Kim et al., 2013; Sato et al., 2014; Wen et al., 2016). Besides, phosphors activated with Mn^{4+} have been recently paid attention due to capability of red emission

using wide variety of host materials (Srivastava and Beers, 1996; Seki et al., 2013; Ye et al., 2013; Sasaki et al., 2014; Wang et al., 2014; Takeda et al., 2015, 2017; Zhou et al., 2016; Cai et al., 2017; Wu et al., 2017; Xi et al., 2017; Zhang et al., 2017; Adachi, 2018; Jansen et al., 2018). Octahedral 6-fold coordination sites are preferred for substitution of Mn^{4+} ions. Fluorides and aluminates are paid much attention as hosts of Mn^{4+}-activated phosphors from the viewpoints of their insulating nature and octahedral sites. Besides, titanates having semiconducting nature are also available for hosts of Mn^{4+}-activated phosphors (Srivastava and Beers, 1996; Seki et al., 2013; Ye et al., 2013; Sasaki et al., 2014; Takeda et al., 2015; Zhang et al., 2017). We have recently reported that double perovskite-type titanates La_2MTiO_6 (M: Mg and Zn) are available as host materials of Mn^{4+}-activated phosphors although a representative perovskite-type titanate $SrTiO_3$ doped with Mn^{4+} could not show any luminescence at room temperature due to significant thermal quenching at low temperature, ∼100 K (Takeda et al., 2015). Low temperature photoluminescence measurements and theoretical band structure calculations have revealed the importance of relative position of Mn 3d orbitals to valence and conduction bands of host materials in order to avoid electron transfer from the valence band to empty t_{2g} orbital of Mn and photoionization. The knowledge obtained from the previous researches encourages us to expand the research target for Mn^{4+}-activated phosphors to Sr_2TiO_4 possessing a K_2MgF_4 type layered perovskite structure. Both $SrTiO_3$ and Sr_2TiO_4 are members in a perovskite family composed of the same constituent elements. $SrTiO_3$ of the representative perovskite-type compound is composed of TiO_6 octahedra sharing corners infinitely, building three-dimensional bulky structure, while Sr_2TiO_4 has layers of the two-dimensional perovskite slab with a single TiO_6 thickness separated by SrO layers as depicted in **Figure 1**. The decreases in structural dimension cause widening band gaps (Reyes-Lillo et al., 2016), which is thought to be a positive factor to suppress the electron transfer and/or the photoionization. Therefore, it is expected that comparison photoluminescence properties between $SrTiO_3$:Mn and Sr_2TiO_4:Mn gives important information to understand the relationship between structural dimension and photoluminescence properties with Mn^{4+}-activation.

In this research, we investigated photoluminescence properties of Mn^{4+}-activated layered perovskite compounds. The differences in photoluminescence properties especially thermal quenching properties between $SrTiO_3$:Mn and Sr_2TiO_4:Mn are discussed from features in crystal structures. In addition, we also investigated into photoluminescence properties of Sr_2ScO_3F:Mn possessing the K_2MgF_4 type structure as well as Sr_2TiO_4:Mn.

EXPERIMENTS

Sample Preparation

All powder samples were synthesized by a solid state reaction method using $SrCO_3$ (Kanto, 99.9%), SrF_2 (Wako, 99.5%), rutile type TiO_2 (Kojundo Chemical, 99.9%), Sc_2O_3 (Shin-Etsu Chemical, 99.99%), and $Mn(NO_3)_2$ $6H_2O$ (Wako, 98.0%) as raw materials. The stoichiometric mixtures of the raw materials were calcined at 1473 K for 5 h in air using alumina crucibles. Where, concentration of Mn substitution was fixed at 0.2 atom% to Ti or Sc. Non-doped samples were also synthesized by the same manner.

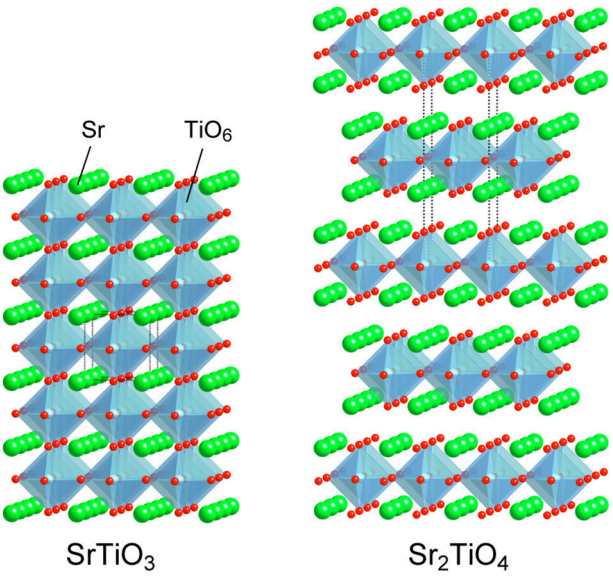

FIGURE 1 | Crystal structures of $SrTiO_3$ and Sr_2TiO_4.

Characterization of Samples

Crystal phases of obtained samples were confirmed by powder X-ray diffraction (XRD) technique (Bruker, D2 Phaser). Photoluminescence measurements were performed using fluorescence spectrometers (Hitachi; F-4500 and Jasco; FP-6500). Photoluminescence spectra were also taken at low temperature (80–300 K with a step of 20 K) using a cryostat (Janis; VPF-475) under vacuum. Diffuse reflectance spectra of non-doped samples were taken by an absorption spectrometer equipping an integration sphere (Shimadzu; UV-3100). The band gaps of the non-doped samples with indirect transition were determined from $(\alpha h\nu)^{1/2}$–$h\nu$ plot, where α, h, and ν represent Kubelka-Munk function, Planck constant, and frequency, respectively.

Band Structure Calculation

The band structures were calculated by the plane wave based density functional theory (DFT) using CASTEP program (Payne et al., 1992; Milman et al., 2000). The Perdew-Burke-Ernzerhof (PBE) functional was used together with the ultrasoft-core potentials (Vanderbilt, 1991; Perdew et al., 1996, 1997). The cutoff energies were set to 300 eV. The electron configurations of the atoms were O: $2s^22p^4$, F: $2s^22p^5$, Sc: $3s^23p^63d^14s^2$, Ti: $3s^23p^63d^24s^2$, Mn: $3d^54s^2$, and Sr: $4s^24p^65s^2$. Super cells of $Sr_{16}Ti_7MnO_{32}$ and $Sr_{16}Sc_7MnO_{25}F_7$ were employed for models of Sr_2TiO_4:Mn and Sr_2ScO_3F:Mn, respectively. Where, one F atom was also replaced with an O atom accompanied by the

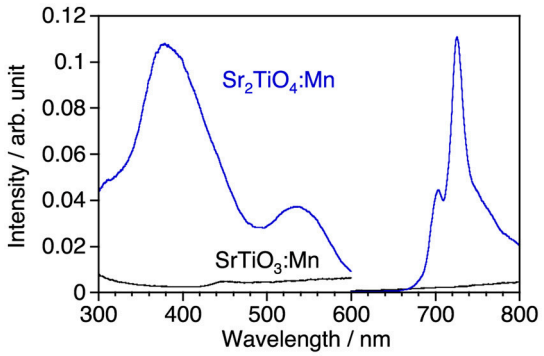

FIGURE 2 | Luminescence spectra of $SrTiO_3$:Mn and Sr_2TiO_4:Mn and corresponding excitation spectra at room temperature. Excitation and monitored wavelengths were 380 and 725 nm, respectively.

substitution of Mn for Sc to maintain the charge balance in the Sr_2ScO_3F:Mn system. From the experimental finding, the local electronic structure for the substituted Mn atom is known to be a 4+ cation, and the Mn ion is in the quintet state. Geometry optimization was carried out with respect to all atomic coordinates.

RESULTS AND DISCUSSION

Luminescence of Sr_2TiO_4:Mn

Figure 2 shows photoluminescence spectra of $SrTiO_3$:Mn and Sr_2TiO_4:Mn with corresponding excitation spectra at room temperature. Sr_2TiO_4:Mn showed deep-red emission with a peak at 725 nm attributed to $^2E_g \rightarrow {}^4A_{2g}$ transition of Mn^{4+} under excitation at 300–580 nm. Although the emission intensity is not high, this is an interesting result taking into consideration of the fact that $SrTiO_3$:Mn shows no emission at room temperature due to significant thermal quenching. Although both strontium titanates are composed of the same elements and are members of the perovskite family, a remarkable difference is present with regard to the structural dimension; Sr_2TiO_4 has a two-dimensional layered structure whereas $SrTiO_3$ has a three-dimensional bulky one. Therefore, the appearance of Mn^{4+}-emission in Sr_2TiO_4:Mn may reflect advantage of the layered perovskite structure in the band structure than bulky one. The further discussion about Sr_2TiO_4:Mn is described later.

Comparison of Luminescence Properties Between Sr_2ScO_3F:Mn and Sr_2TiO_4:Mn

Although, as shown in **Figure 3A**, Sr_2TiO_4 has a wider band gap (3.46 eV) than $SrTiO_3$ (3.21 eV) as reported in literature (Reyes-Lillo et al., 2016), other layered perovskite compounds possessing wider band gaps are preferred for efficient Mn^{4+}-emission because of less probability of the electron transfer between Mn 3d and the valence and/or conduction band. Strontium scandium oxyfluoride Sr_2ScO_3F with a K_2MgF_4 type structure as well as Sr_2TiO_4, which has been recently discovered (Wang et al., 2015), was thought to be a good candidate because its octahedral building unit ScO_5F based on the optically inert rare earth

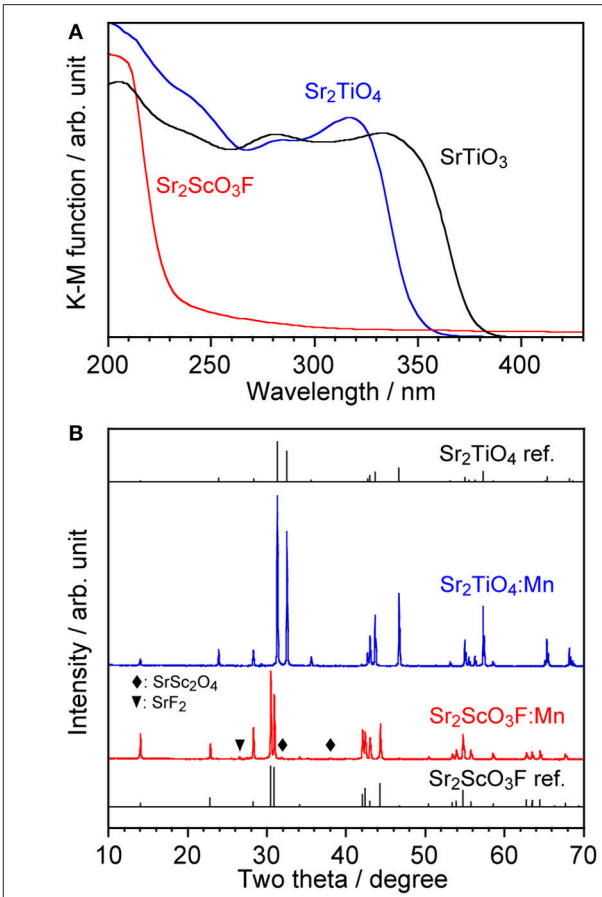

FIGURE 3 | (A) Diffuse reflectance spectra of non-doped Sr_2TiO_4, Sr_2ScO_3F, and $SrTiO_3$ and **(B)** XRD patterns of Sr_2TiO_4:Mn and Sr_2ScO_3F:Mn with reference patterns.

element was expected to give a wider energy gap in comparison with TiO_6. XRD confirmed that Sr_2ScO_3F:Mn was obtained as the almost pure phase of Sr_2ScO_3F although it contained tiny amounts of SrF_2 and $SrSc_2O_4$ as impurities whereas Sr_2TiO_4:Mn was obtained as a pure phase without any impurities (**Figure 3B**). Relative intensities of diffraction peaks of Sr_2ScO_3F:Mn at 14.1, 28.3, 43.0, and 58.5 degrees corresponding to reflections from (002), (004), (006), and (008), respectively, were remarkably strong in comparison with the standard ones due to orientation of crystals in (00*l*). The band gap of Sr_2ScO_3F has been discovered to be 5.38 eV, being wider than that of Sr_2TiO_4 (**Figure 3A**). **Figure 4** shows emission and excitation spectra of Sr_2ScO_3F:Mn and Sr_2TiO_4:Mn at room temperature. Sr_2ScO_3F:Mn showed deep-red emission owing to transition of Mn^{4+} giving a peak at 697 nm. Obvious two excitation bands in 300–460 nm and in 480–580 nm are attributed to spin-allow $^4A_{2g} \rightarrow {}^4T_{1g}$ and $^4A_{2g} \rightarrow {}^4T_{2g}$ transition of Mn^{4+} ions, respectively, while a weak excitation band owing to spin-forbidden $^4A_{2g} \rightarrow {}^2T_{2g}$ transition is difficult to distinguish and it may be embedded in the tail of the $^4A_{2g} \rightarrow {}^4T_{1g}$ band as observed in other titanates and tantalates (Sasaki et al., 2014; Wang et al., 2014; Takeda et al., 2015, 2017). Interestingly, the emission from Sr_2ScO_3F:Mn was

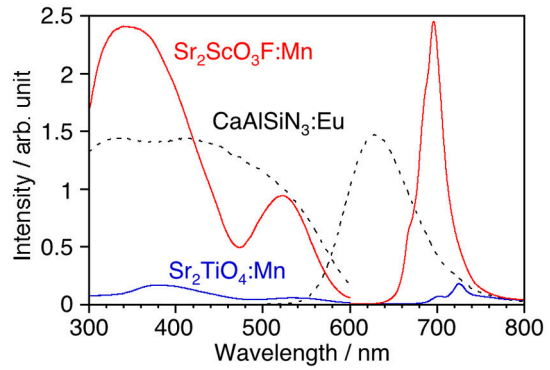

FIGURE 4 | Luminescence spectra of Sr_2TiO_4:Mn, Sr_2ScO_3F:Mn, and $CaAlSiN_3$:Eu with corresponding excitation spectra at room temperature. Excitation and monitored wavelengths were 380 and 725 nm for Sr_2TiO_4:Mn, 345 and 697 nm for Sr_2ScO_3F:Mn, and 340 and 630 nm for $CaAlSiN_3$:Eu.

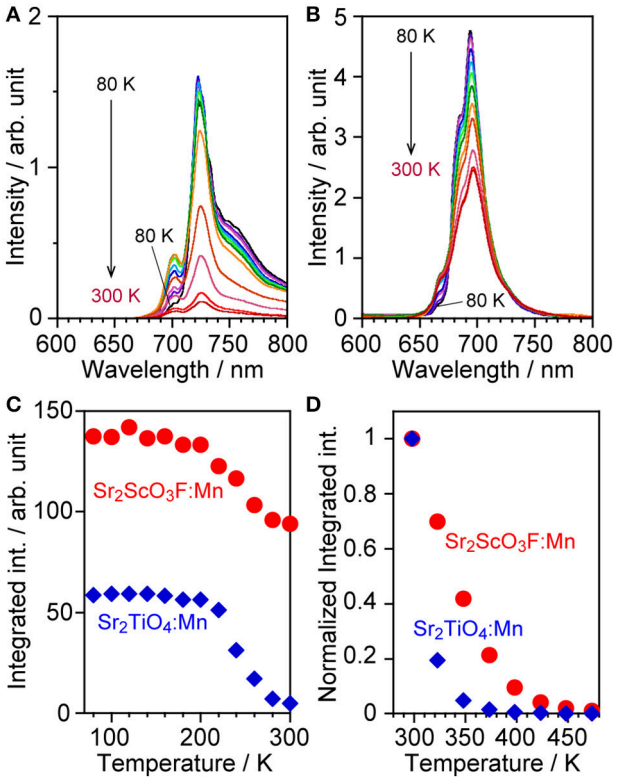

FIGURE 5 | Emission spectra of **(A)** Sr_2TiO_4:Mn and **(B)** Sr_2ScO_3F:Mn at low temperature (80–300 K), **(C)** relative integrated emission intensity of them, and **(D)** normalized integrated emission intensity of Sr_2TiO_4:Mn and Sr_2ScO_3F:Mn at high temperature (298–473 K). Excitation wavelengths were 380 and 340–345 nm for Sr_2TiO_4:Mn and Sr_2ScO_3F:Mn, respectively.

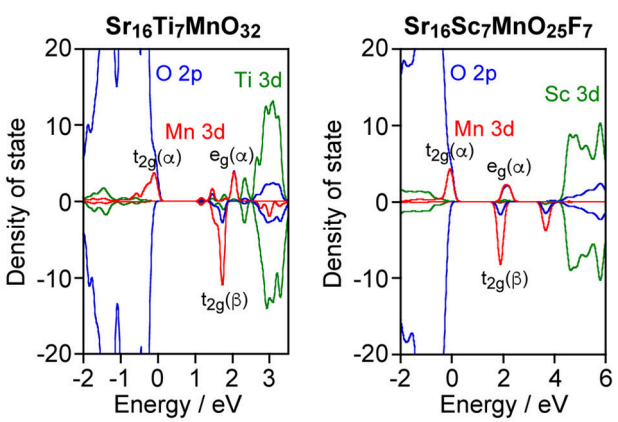

FIGURE 6 | PDOS of $Sr_{16}Ti_7MnO_{32}$ and $Sr_{16}Sc_7MnO_{25}F_7$.

much stronger than that from Sr_2TiO_4:Mn; the internal and external quantum yields of Sr_2ScO_3F:Mn excited at 345 nm at room temperature (50.5 and 43.5%) were much higher than those of Sr_2TiO_4:Mn excited at 380 nm (3.4 and 2.5%). The Mn^{4+}-emission from fluoride hosts consists of some very sharp lines while that from oxide hosts is broad (Zhou et al., 2016; Adachi, 2018). The emission from Sr_2ScO_3F:Mn is broad as well as Mn^{4+}-activated oxide phosphors despite presence of the Sc-F bond. This means that influences of F upon the photoluminescence property of Sr_2ScO_3F:Mn are not significant. In Sr_2ScO_3F:Mn, it is preferred from the charge compensation that one fluorine is replaced with one oxygen when Mn^{4+} is substituted for Sc^{3+}. Such co-substitution results in the formation of MnO_6 octahedra which give broad Mn^{4+}-emission. The spectra of $CaSiAlN_3$:Eu, which is the representative red-emitting phosphor activated with Eu^{2+}, are also shown in **Figure 4**. The Sr_2ScO_3F:Mn emission is sharper and stronger than the $CaSiAlN_3$:Eu emission however the wavelength of the Sr_2ScO_3F:Mn emission is excessively long, that is, almost the half portion of emission is located in the invisible region ($\lambda > 700$ nm). $CaAlSiN_3$:Eu can be excited by blue-LEDs ($\lambda = 450$–470 nm) more efficiently than Sr_2ScO_3F:Mn while Sr_2ScO_3F:Mn can be excited by near ultraviolet LEDs ($\lambda = 350$–400 nm) more efficiently than $CaAlSiN_3$:Eu.

Measurements of thermal quenching were performed at low (80–300 K) and high temperature ranges (298–473 K). Both samples suffered temperature quenching even in the low temperature range especially higher than 200 K as shown in **Figures 5A–C**. The maximum peak intensity decreased as measurement temperature rose while the emission of anti-Stokes sidebands, which were observed in regions shorter than 710 and 675 nm in Sr_2TiO_4:Mn and Sr_2ScO_3F:Mn, respectively, was enhanced due to transition of excited electrons to upper vibration states by thermal energy (Wu et al., 2017; Adachi, 2018). It results in the non-obvious decreases in the integrated emission intensity up to 200 K. Sr_2ScO_3F:Mn exhibited stronger emission than Sr_2TiO_4:Mn at all temperatures, moreover, the intensity of Sr_2TiO_4:Mn at 80 K was lower than that of Sr_2ScO_3F:Mn at 300 K. Thus, Sr_2TiO_4:Mn exhibited more remarkable thermal quenching in comparison with Sr_2ScO_3F:Mn. In the high temperature range (298–473 K), significant thermal quenching occurred in both samples as shown in **Figure 5D**, however Sr_2ScO_3F:Mn showed lesser thermal quenching than Sr_2TiO_4:Mn. At 373 K, Sr_2ScO_3F:Mn showed 20% of emission intensity in comparison with that at 298 K whereas emission from Sr_2TiO_4:Mn was completely quenched.

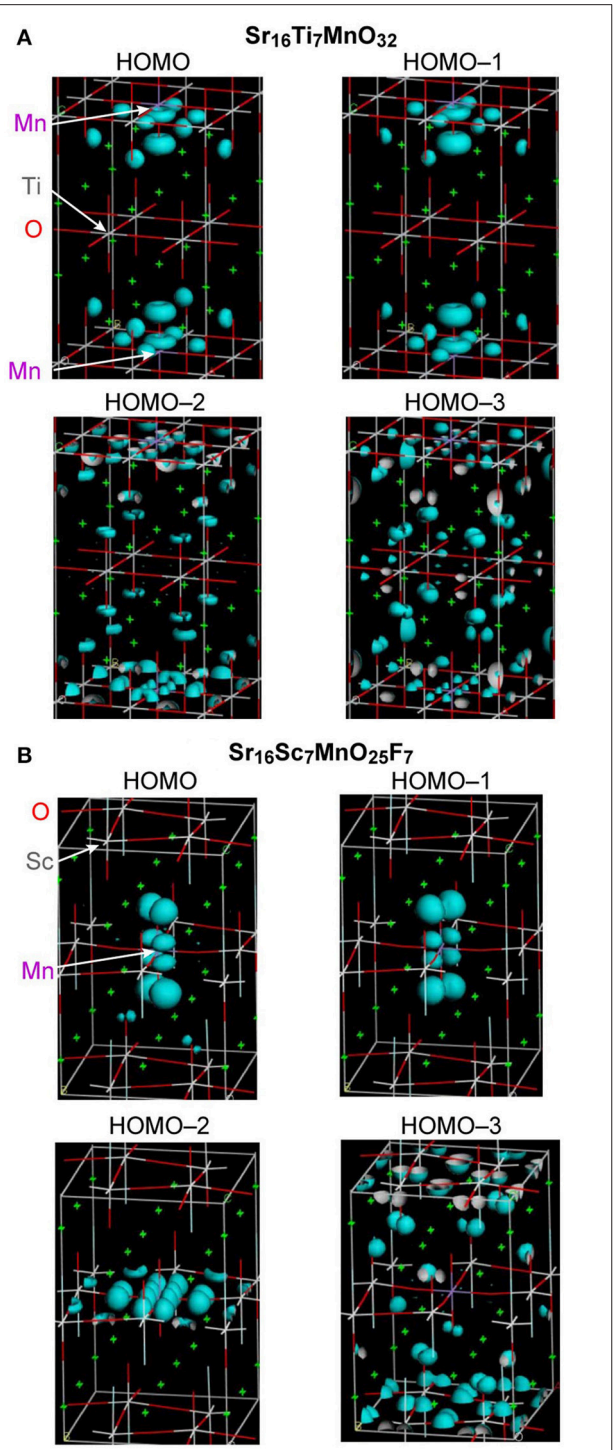

FIGURE 7 | Electron density contour maps of top four occupied orbitals for **(A)** $Sr_{16}Ti_7MnO_{32}$ and **(B)** $Sr_{16}Sc_7MnO_{25}F_7$.

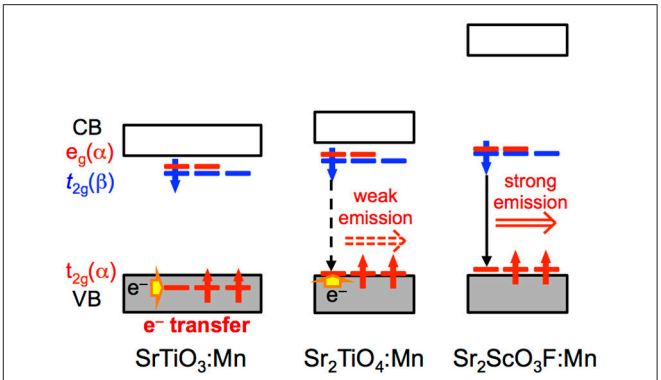

FIGURE 8 | Proposed mechanism for $SrTiO_3$:Mn, Sr_2TiO_4:Mn, and Sr_2ScO_3F:Mn.

Band Structures of Sr_2TiO_4:Mn and Sr_2ScO_3F:Mn

As described above, Sr_2ScO_3F:Mn showed superior characteristics, that is, higher emission intensity and lesser thermal quenching, to Sr_2TiO_4:Mn. Relative position of Mn 3d orbitals to the valence and conduction bands of host materials is an important factor for Mn^{4+}-activated phosphors as we have reported previously (Takeda et al., 2015, 2017). Therefore, band structures of Sr_2TiO_4:Mn and Sr_2ScO_3F:Mn were investigated by the DFT method. **Figure 6** depicts projected density of states (PDOS) near the band gap of $Sr_{16}Ti_7MnO_{32}$ and $Sr_{16}Sc_7MnO_{25}F_7$ corresponding to Sr_2TiO_4:Mn and Sr_2ScO_3F:Mn. In **Figure 6**, positive and negative values in DOS represent DOS for up-spin (α) and down-spin (β) electrons, respectively, and 0 eV of energy represents the Fermi level. In Sr_2TiO_4:Mn, the valence and conduction bands of host are composed of O 2p and Ti 3d orbitals, respectively, like $SrTiO_3$:Mn. In PDOS of Sr_2TiO_4:Mn, the $t_{2g}(\alpha)$ orbitals of Mn look to be located slightly higher position than the valence band however a tail of $t_{2g}(\alpha)$ is embedded in the valence band. The DFT calculation reveals that Sr_2TiO_4:Mn has absolutely different feature in the relative position of Mn 3d orbitals to the valence band from $SrTiO_3$:Mn, in which the $t_{2g}(\alpha)$ orbitals are deeply embedded in the valence band (Takeda et al., 2015). Although a part of $t_{2g}(\alpha)$ orbitals is located in positive energy region, it doesn't indicate the presence of empty $t_{2g}(\alpha)$ orbitals. The total numbers of electrons calculated for both $Sr_{16}Ti_7MnO_{32}$ and $Sr_{16}Sc_7MnO_{25}F_7$ models were 443. In the quintet state, the numbers of occupied orbitals should be 223 and 220 for α- and β-electrons, respectively. If the top of $t_{2g}(\alpha)$ orbital of Mn 3d is empty, the lowest unoccupied molecular orbital for α-electron (#224 α-orbital) should be Mn 3d located near 0 eV. However, #224 α-orbital is not Mn 3d located around 0 eV but Mn3d orbital below the conduction band [indicated as $e_g(\alpha)$ in **Figure 6**] in both models. The small portion of the occupied orbitals beyond the Fermi level observed in PDOS is due to broadening of energy widths of orbitals by the smearing treatment in the process of PDOS creation. Thus, it has been confirmed that all Mn 3d orbitals around 0 eV are occupied ones. The PDOS of Sr_2ScO_3F:Mn shows that the $t_{2g}(\alpha)$ orbitals of Mn is located slightly higher position than the valence band without tailing portion at a lower energy side. The electron density contour maps for

top four occupied molecular orbitals including the highest occupied molecular orbital (HOMO) are compared to see details of the differences between Sr_2TiO_4:Mn and Sr_2ScO_3F:Mn (**Figure 7**). In Sr_2ScO_3F:Mn, contribution of the occupied Mn 3d orbitals is seen only in the top three occupied orbitals (from HOMO to HOMO−2) and the forth highest occupied orbital (HOMO−3) is composed of only O 2p orbital. On the other hand, small contribution of the Mn 3d orbital is also seen in HOMO−3 of Sr_2TiO_4:Mn although Mn 3d orbitals mainly contribute to top three occupied orbitals. If hybridization between O 2p and $t_{2g}(\alpha)$ of Mn 3d is small, the occupied Mn 3d orbitals appear in only three orbitals. The appearance of Mn 3d in four orbitals in Sr_2TiO_4:Mn (from HOMO to HOMO−3) indicates stronger hybridization between O 2p and Mn 3d than Sr_2ScO_3F:Mn. It is also noticed in PDOS that energy gap between $e_g(\alpha)$ of Mn 3d and the bottom of conduction band is larger in Sr_2ScO_3F:Mn than Sr_2TiO_4:Mn. It reflects the remarkably wider band gap of Sr_2ScO_3F than Sr_2TiO_4.

Figure 8 illustrates proposed mechanism based on photoluminescence measurements and band structure calculations for Mn^{4+}-activated $SrTiO_3$, Sr_2TiO_4, and Sr_2ScO_3F. The most significant difference in photoluminescence property between Sr_2TiO_4:Mn and $SrTiO_3$:Mn is the appearance of Mn^{4+}-emission in Sr_2TiO_4:Mn at room temperature. The difference in the relative position of $t_{2g}(\alpha)$ orbitals of Mn between $SrTiO_3$:Mn and Sr_2TiO_4:Mn is of importance in explanation for the appearance of Mn^{4+}-emission in Sr_2TiO_4:Mn. In $SrTiO_3$:Mn, the $t_{2g}(\alpha)$ orbitals embedded in the valence band facilitate thermal quenching via the electron transfer from the valence band to the empty t_{2g} in the excited state ^2E_g, resulting in low quenching temperature, ∼100 K (Takeda et al., 2015). In contrast to $SrTiO_3$:Mn, $t_{2g}(\alpha)$ in Sr_2TiO_4:Mn is located slightly higher position than the valence band. Therefore, Sr_2TiO_4:Mn shows Mn^{4+}-emission even at room temperature. Interaction between TiO_6 octahedra may affect the relative position of $t_{2g}(\alpha)$ orbitals of Mn. Each TiO_6 octahedron connects to six TiO_6 octahedra in $SrTiO_3$ while TiO_6 connects to four TiO_6 octahedra in the perovskite slab in Sr_2TiO_4 as shown in **Figure 1**, indicating that degree of energy delocalization is higher in three-dimensional $SrTiO_3$ than two-dimensional Sr_2TiO_4. The smaller interaction between TiO_6 octahedra may cause less interaction between O 2p and occupied of Mn 3d orbitals, that is, $t_{2g}(\alpha)$ orbitals. Thus, the advantage of two-dimensional layered perovskite structure for Mn^{4+}-activated phosphors can be explained by the smaller interaction of MO_6 octahedra. Such discussion can be applied to another Mn^{4+}-activated titanate phosphor La_2MgTiO_6:Mn with a B-site ordered double perovskite structure, which is an efficient Mn^{4+}-activated phosphor with 58.7% of an internal quantum yield (Takeda et al., 2015). In La_2MgTiO_6, each TiO_6 octahedron is surrounded by six MgO_6 octahedra, meaning that TiO_6 is isolated from other TiO_6 octahedra even though the perovskite-type structure (Lee et al., 2000). Thus, the structure of La_2MgTiO_6 can be regarded as a quasi-zero-dimensional structure with respect to the connection between TiO_6 octahedra. The less interaction of TiO_6 in La_2MgTiO_6:Mn leads the larger energy gap between the valence band and $t_{2g}(\alpha)$ of Mn, resulting in the superior photoluminescence efficiency to Sr_2TiO_4:Mn. In Sr_2ScO_3F:Mn, the $t_{2g}(\alpha)$ orbitals of Mn 3d are located above the valence band with a slightly larger energy gap than Sr_2TiO_4:Mn due to the small hybridization between O 2p and Mn 3d as described above. On the other hand, the larger energy gap between $e_g(\alpha)$ and the bottom of conduction band in Sr_2ScO_3F:Mn suppresses quenching via photoionization, in which an electron in $e_g(\alpha)$ orbitals in the excited state is transferred to the conduction band and then is relaxed without emission (Takeda et al., 2017). Thus, the two factors, the less interaction between $t_{2g}(\alpha)$ and the valence band and the large energy gap between $e_g(\alpha)$ and the bottom of conduction band, positively affect the smaller thermal quenching in Sr_2ScO_3F:Mn than Sr_2TiO_4:Mn, resulting in the stronger emission.

CONCLUSIONS

Photoluminescence properties of Mn^{4+}-activated strontium titanates, $SrTiO_3$:Mn with three-dimensional bulky perovskite structure and Sr_2TiO_4:Mn with two-dimensional layered perovskite structure, have been compared in this research. Sr_2TiO_4:Mn shows Mn^{4+}-emission even at room temperature despite no emission from $SrTiO_3$:Mn. In addition, the results in our systematic research suggest that the less interaction between MO_6 octahedra of B-site cation in the perovskite family provides positive influences in Mn^{4+}-emission. Comparison between Sr_2TiO_4:Mn and Sr_2ScO_3F:Mn indicates that ScO_5F octahedra are preferable constituents to TiO_6 ones for the Mn^{4+}-activated phosphors. Thus, the present research demonstrates that scandium, which is one of optically inert rare earth elements, is a useful element as a major constituent for design of Mn^{4+}-activated phosphors.

AUTHOR CONTRIBUTIONS

HidK managed all experiments and wrote the manuscript. YT performed experiments on synthesis of samples and evaluation of photoluminescence properties of them. HisK performed band structure calculations. MakK and MasK planned experiments and made discussion about the results.

FUNDING

This research was partly supported by KAKENHI Grant Numbers JP16H06438 and JP16H06439 in Scientific Research on Innovative Area Mixed Anion and JP16H02391 in Scientific Research (A) and Dynamic Alliance for Open Innovation Bridging Human, Environment and Materials in Network Joint Research Center for Materials and Devices.

REFERENCES

Adachi, S. (2018). Photoluminescence properties of Mn^{4+}-activated oxide phosphors for use in white-LED applications: a review. *J. Lumin.* 202, 263–281. doi: 10.1016/j.jlumin.2018.05.053

Cai, P., Qin, L., Chen, C., Wang, J., and Seo, H. J. (2017). Luminescence, energy transfer and optical thermometry of a novel narrow red emitting phosphor: $Cs_2WO_2F_4:Mn^{4+}$. *Dalton Trans.* 46, 14331–14340. doi: 10.1039/C7DT02751F

Daicho, H., Iwasaki, T., Enomoto, K., Sasaki, Y., Maeno, Y., Shinomiya, Y., et al. (2012). A novel phosphor for glareless white light-emitting diodes. *Nat. Commun.* 3:1132. doi: 10.1038/ncomms2138

Daicho, H., Shinomiya, Y., Enomoto, K., Nakano, A., Sawa, H., Matsuishi, S., et al. (2018). A novel red-emitting $K_2Ca(PO_4)F:Eu^{2+}$ phosphor with a large Stokes shift. *Chem. Commun.* 54, 884–887. doi: 10.1039/C7CC08202A

Jansen, T., Jüstel, T., Kirm, M., Vielhauer, S., Khaidukov, N. M., and Makhovd, V. N. (2018). Composition dependent spectral shift of Mn^{4+} luminescence in silicate garnet hosts $CaY_2M_2Al_2SiO_{12}$ (M = Al, Ga, Sc). *J. Lumin.* 198, 314–319. doi: 10.1016/j.jlumin.2018.02.054

Kim, S. W., Hasegawa, T., Ishigaki, T., Uematsu, K., Toda, K., and Sato, M. (2013). Efficient red emission of blue-light excitable new structure type $NaMgPO_4:Mn^{4+}$ phosphor. *ECS Solid State Lett.* 2, R49–R51. doi: 10.1149/2.004312ssl

Lee, D.-Y., Yoon, S.-J., Yeo, J.-H., Nahm, S., Paik, J. H., Whang, K.-C., et al. (2000). Crystal structure and microwave dielectric properties of $La(Mg_{1/2}Ti_{1/2})O_3$ ceramics. *J. Mater. Sci. Lett.* 19, 131–134. doi: 10.1023/A:1006603615193

Li, H.-L., Xie, R.-J., Hirosaki, N., Takeda, T., and Zhou, G. H. (2009). Synthesis and luminescence properties of orange–red-emitting $M_2Si_5N_8:Eu^{2+}$ (M = Ca, Sr, Ba) light-emitting diode conversion phosphors by a simple nitridation of MSi_2. *Int. J. Appl. Ceram. Technol.* 6, 459–464. doi: 10.1111/j.1744-7402.2009.02370.x

Li, Y. Q., Steen, J. E. J., Krevel, J. W. H., Botty, G., Delsing, A. C. A., DiSalvo, F. J., et al. (2006). Luminescence properties of red-emitting $M_2Si_5N_8:Eu^{2+}$ (M = Ca, Sr, Ba) LED conversion phosphors. *J. Alloys Compd.* 417, 273–279. doi: 10.1016/j.jallcom.2005.09.041

Lin, Y. C., Karlsson, M., and Bettinelli, M. (2016). Inorganic phosphor materials for lighting. *Top. Curr. Chem.* 374:21. doi: 10.1007/s41061-016-0023-5

Milman, V., Winkler, B., White, J. A., Pickard, C. J., Payne, M. C., Akhmatskaya, E. V., et al. (2000). Electronic structure, properties, and phase stability of inorganic crystals: a pseudopotential plane-wave study. *Int. J. Quan. Chem.* 77, 895–910. doi: 10.1002/(SICI)1097-461X(2000)77:5<895::AID-QUA10>3.0.CO;2-C

Payne, M. C., Teter, M. P., Allan, D. C., Arias, T. A., and Johnnopoulos, J. D. (1992). Iterative minimization techniques for *ab initio* total-energy calculations: molecular dynamics and conjugate gradients. *Rev. Mod. Phys.* 64, 1045–1097. doi: 10.1103/RevModPhys.64.1045

Perdew, J. P., Burke, K., and Ernzerhof, M. (1996). Generalized gradient approximation made simple. *Phys. Rev. Lett.* 77, 3865–3868. doi: 10.1103/PhysRevLett.77.3865

Perdew, J. P., Burke, K., and Ernzerhof, M. (1997). Generalized gradient approximation made simple. *Phys. Rev. Lett.* 77, 3865–3868. doi: 10.1103/PhysRevLett.78.1396

Reyes-Lillo, S. E., Rangel, T., Bruneval, F., and Neaton, J. B. (2016). Effects of quantum confinement on excited state properties of $SrTiO_3$ from *ab initio* many-body perturbation theory. *Phys. Rev. B* 94:041107. doi: 10.1103/PhysRevB.94.041107

Sasaki, T., Fukushima, J., Hayashi, Y., and Takizawa, H. (2014). Synthesis of photoluminescence properties of Mn^{4+}-doped $BaMg_6Ti_6O_{19}$ phosphor. *Chem. Lett.* 43, 1061–1063. doi: 10.1246/cl.140282

Sato, Y., Kato, H., Kobayashi, M., Masaki, T., Yoon, D.-H., and Kakihana, M. (2014). Tailoring of deep-red luminescence in $Ca_2SiO_4:Eu^{2+}$. *Angew. Chem. Int. Ed.* 53, 7756–7759. doi: 10.1002/anie.201402520

Seki, K., Kamei, S., Uematsu, K., Ishigaki, T., Toda, K., and Sato, M. (2013). Enhancement of the luminescence efficiency of $Li_2TiO_3:Mn^{4+}$ red emitting phosphor for white LEDs. *J. Ceram. Process. Res.* 14, s67–s70.

Srivastava, A. M., and Beers, W. W. (1996). Luminescence of Mn^{4+} in the distorted perovskite Gd_2MgTiO_6. *J. Electrochem. Soc.* 143, L203–L205. doi: 10.1149/1.1837087

Takeda, Y., Kato, H., Kobayashi, M., Kobayashi, H., and Kakihana, M. (2015). Photoluminescence properties of Mn^{4+}-activated perovskite-type titanates, $La_2MTiO_6:Mn^{4+}$ (M = Mg and Zn). *Chem. Lett.* 44, 1541–1543. doi: 10.1246/cl.150748

Takeda, Y., Kato, H., Kobayashi, M., Nozawa, S., Kobayashi, H., and Kakihana, M. (2017). Photoluminescence properties of double perovskite tantalates activated with Mn^{4+}, $AE_2LaTaO_6:Mn^{4+}$ (AE = Ca, Sr, and Ba). *J. Phys. Chem. C* 121, 18837–18844. doi: 10.1021/acs.jpcc.7b06280

Toda, K., Kawakami, Y., Kousaka, S., Ito, Y., Komeno, A., Uematsu, K., et al. (2006). New silicate phosphors for a white LED. *IEICE Trans. Electoron.* E89–C, 1406–1412.

Tsai, Y. T., Chiang, C. Y., Zhou, W., Lee, J. F., Sheu, H. S., and Liu, R. S. (2015). Structural ordering and charge variation induced by cation substitution in $(Sr,Ca)AlSiN_3:Eu$ phosphor. *J. Am. Chem. Soc.* 137, 8936–8939. doi: 10.1021/jacs.5b06080

Uheda, K., Hirosaki, N., Yamamoto, Y., Naito, A., Nakajima, T., and Yamamoto, H. (2006). Luminescence properties of a red phosphor, $CaAlSiN_3:Eu^{2+}$, for white light-emitting diodes, *Electrochem. Solid State Lett.* 9, H22–H25. doi: 10.1149/1.2173192

Vanderbilt, D. (1991). Implementation of ultrasoft pseudopotentials in *ab initio* molecular dynamics. *Phys. Rev. B* 43, 6796–6799. doi: 10.1103/PhysRevB.43.6796

Wang, L., Xie, R. J., Suehiro, T., Takeda, T., and Hirosaki, N. (2018). Down-conversion nitride materials for solid state lighting: recent advances and perspectives. *Chem. Rev.* 118, 1951–2009. doi: 10.1021/acs.chemrev.7b00284

Wang, L., Yuan, L., Xu, Y., Zhou, R., Qu, B., Ding, N., et al. (2014). Luminescent properties of $LaLiTaO_6:Mn^{4+}$ and its application as red emission LEDs phosphor. *Appl. Phys. A: Mater. Sci. Process.* 117, 1777–1783. doi: 10.1007/s00339-014-8827-z

Wang, Y., Tang, K., Zhu, B., Wang, D., Hao, Q., and Wang, Y. (2015). Synthesis and structure of a new layered oxyfluoride Sr_2ScO_3F with photocatalytic property. *Mater. Res. Bull.* 65, 42–46. doi: 10.1016/j.materresbull.2015.01.042

Watanabe, H., and Kijima, N. (2009). Crystal structure and luminescence properties of $Sr_xCa_{1-x}AlSiN_3:Eu^{2+}$ mixed nitride phosphors. *J. Alloy Compd.* 475, 434–439. doi: 10.1016/j.jallcom.2008.07.054

Wen, D., Kuwahara, H., Kato, H., Kobayashi, M., Sato, Y., Masaki, T., et al. (2016). Anomalous orange light-emitting $(Sr,Ba)_2SiO_4:Eu^{2+}$ phosphors for warm white LEDs. *ACS Appl. Mater. Interfaces* 8, 11615–11620. doi: 10.1021/acsami.6b02237

Wu, W.-L., Fang, M.-H., Zhou, W., Lesniewski, T., Mahlik, S., Grinberg, M., et al. (2017). High color rendering index of $Rb_2GeF_6:Mn^{4+}$ for light-emitting diodes. *Chem. Mater.* 29, 935–939. doi: 10.1021/acs.chemmater.6b05244

Xi, L., Pan, Y., Zhu, M., Lian, H., and Lin, J. (2017). Room-temperature synthesis and optimized photoluminescence of a novel red phosphor $NaKSnF_6:Mn^{4+}$ for application in warm WLEDs. *J. Mater. Chem. C* 5, 9255–9263. doi: 10.1039/C7TC02996A

Ye, T., Li, S., Wu, X., Xu, M., Wei, X., Wang, K., et al. (2013). Sol-gel preparation of efficient red phosphor $Mg_2TiO_4:Mn^{4+}$ and XAFS investigation on the substitution of Mn^{4+} for Ti^{4+}. *J. Mater. Chem. C* 1, 4327–4333. doi: 10.1039/C3TC30553H

Zhang, S., Hu, Y., Duan, H., Fu, Y., and He, M. (2017). An efficient, broad-band red-emitting $Li_2MgTi_3O_8:Mn^{4+}$ phosphor for blue-converted white LEDs. *J. Alloys Compd.* 693, 315–325. doi: 10.1016/j.jallcom.2016.09.203

Zhou, Z., Zhou, N., Xia, M., Yokoyama, M., and Hintzen, H. T. (2016). Research progress and application prospects of transition metal Mn^{4+}-activated luminescent materials. *J. Mater. Chem. C* 4, 9143–9161. doi: 10.1039/c6tc02496c

Conflict of Interest Statement: The authors declare that the research was conducted in the absence of any commercial or financial relationships that could be construed as a potential conflict of interest.